

Rheology and Structure of Lithium-Ion Battery Electrode Slurries

Carl D. Reynolds,* Sam D. Hare, Peter R. Slater, Mark J. H. Simmons, and Emma Kendrick

The rheology of electrode slurries dictates the final coating microstructure. High slurry viscosity creates excess pressure and limits coating speed, elasticity causes instabilities leading to coating defects and high flow causes slumping leading to thin, poorly structured coatings. However, due to differing solvent systems and components, and the complex nature of the many competing interactions, finding the source of these detrimental rheological properties can be difficult. Herein, a systematic rheological characterization of all components of an industrially relevant anode and cathode slurry is presented. Through a combinatorial approach, the additive nature of the interactions is explored, using steady shear, small and large amplitude oscillatory shear to give insight into the underlying structure, which is vital to develop novel, more sustainable formulations. For water-based anodes, the polymeric binder dictates the rheology, thickening the slurry, allowing efficient suspension of the active material particles, which only contribute an increase in viscosity. For N-methyl pyrrolidine (NMP)-based cathodes, the conductive additive forms a weakly gelled network in NMP which flows under coating shear. The binder, as well as thickening, also functions to adsorb to active material surfaces, displacing additive and leaving it free to form this network, which is key to the electronic properties of the dried electrode.

1. Introduction

Lithium-ion battery electrodes are manufactured in several stages. Materials are mixed into a slurry, which is then coated onto a foil current collector, dried, and calendared (compressed). The final coating is optimized for electronic conductivity through the solid content of the electrode, and for ionic conductivity through the electrolyte-filled pore structure and the active material. This microstructure is the result of the slurry dispersion, deposition, and drying of the coating.^[1,2] There are a multitude of variables in this multi-stage process, and thus monitoring and understanding the process at each stage is highly important to optimize manufacturing for best performance and reduce wastage. There exist a range of metrology options for coating drying and the final electrochemical properties, but inspection at the slurry stage, after mixing, is limited.^[2,3]

The components of an electrode coating include the active material, which is a lithium-containing material for the cathode

such as lithium nickel manganese cobalt oxides (NMCs), or for the anode, a material that can accommodate lithium, commonly graphite (GRA) is used. They also include a conductive additive, which is used to form a conducting network throughout the coating. Commonly carbon black (CB) is used, however, alternatives such as carbon nanotubes, graphene, and small particle size graphite can also be used to optimize the electronic conductivity.^[4,5] A binder is also required, polymeric additives which aid with particle dispersion in the slurry, improve adhesion to the current collector, add flexibility to the coating and form a cohesive bond between the active material particles. It is thought that the conductive additive is suspended within the polymer matrix, and it is this carbon-binder domain that forms the 3D conductivity within the electrode coating after drying.^[6]


The sustainability of the process depends heavily upon the solvent used to disperse the slurry.^[7,8] Water-based slurries are preferred due to the toxicity of alternatives, and the lower cost. A mixture of carboxymethyl cellulose (CMC) and styrene butadiene rubber (SBR) is a common binder common for water-based slurries (e.g., graphite slurries are processed in this way industrially). For N-methyl pyrrolidine (NMP) slurries, polyvinylidene fluoride (PVDF) is frequently used, which is still

C. D. Reynolds, E. Kendrick
School of Metallurgy and Materials
University of Birmingham
Birmingham B15 2SE, UK
E-mail: c.d.reynolds@bham.ac.uk

C. D. Reynolds, S. D. Hare, P. R. Slater, M. J. H. Simmons, E. Kendrick
Faraday Institution
Didcot OX11 0RA, UK

S. D. Hare, M. J. H. Simmons
School of Chemical Engineering
University of Birmingham
Birmingham B15 2TT, UK

P. R. Slater
School of Chemistry
University of Birmingham
Birmingham B15 2TT, UK

 The ORCID identification number(s) for the author(s) of this article can be found under <https://doi.org/10.1002/ente.202200545>.

© 2022 The Authors. Energy Technology published by Wiley-VCH GmbH. This is an open access article under the terms of the Creative Commons Attribution License, which permits use, distribution and reproduction in any medium, provided the original work is properly cited.

DOI: 10.1002/ente.202200545

the main industrial processing route for NMC cathodes. The amount of solvent is also key to sustainability as higher amounts require longer, more energy-intensive drying, hence high-weight solid slurries are generally preferred.

All these components are dispersed in the solvent in the mixing stage, forming a slurry. This is then coated onto a foil current collector, dried, and calendared (compressed) to form the electrode. The microstructure of this electrode is key to the final electronic properties,^[9] and has been shown to be highly dependent on the processing in each step, e.g., coating technique,^[10] drying temperatures,^[3,11] calendaring.^[12,13] It is therefore important to employ metrology at each stage, to gain understanding and enable modeling approaches, digital twins of the process, and in-line manufacturing control.^[2,14–16]

Due to the complexity of the process and the number of variables involved, measuring the properties of the electrode slurry can be highly informative to optimize later steps, detect failures early, and prevent wastage. Rheology is one such tool that can be used to study the slurry structure and extract information after the mixing stage.

Rheology is dictated by the formulation and the interactions of each component in the mixture, and thus can be used to study different formulations and compare new ingredients and additives. For example, surfactants are sometimes added to better disperse components, the effectiveness of this can be monitored in the flow properties.

The interactions in the slurry are highly dependent on the mixing step, so rheology can also be used to evaluate the mixing effectiveness. For example, more intensive mixing disperses and deagglomerates the materials, leading to small particle sizes, which often leads to lower overall viscosity. Rheology is also sensitive to the presence of network structures and so can be used to detect the optimal slurry structure—a network of conductive additives spanning the bulk to give conductivity in the dry coating.

Rheology is also a key factor in predicting performance in the subsequent coating stage, for example, high viscosities cause high pressure in the coater and can limit coating speed, elastic behavior can cause coating instability and low viscosity, the highly flowing slurry will spread and slump after coating. Therefore, rheology could be used for quality control by defining a tight set of criteria for an optimal coating on an existing line, or to adapt coating settings (e.g., speed, thickness) to obtain uniform coatings from a new formulation.

For these reasons, rheology is an ideal metrology option for gaining insight at the slurry stage, with the final objective of being able to predict the electrode properties from the slurry, coating and drying parameters, and to be able to control the process in real time.^[14] Understanding the initial rheological properties could help to reduce the need for further electrode coatings and testing, thus reducing the time for new cell developments and time to market.^[2,3]

To make predictions about the coating behavior, we must understand the deformations in the coater and compare them to the rheological measurement. In a blade coater, the shear rate for a Newtonian fluid during coating can be given by^[17]

$$\dot{\gamma} = \frac{v}{h} \quad (1)$$

where v = coating speed and h = coating gap. Electrode slurries are not Newtonian, and may show shear thinning and yield stress behavior. Maillard et al.^[18] observed yield stress fluids in a blade coater and found that a uniform shear region was formed between the material built up behind the blade and material close to the substrate. This region was larger than the coating gap so the steady state shear rate was lower than that predicted by Equation (1). Hence, it is reasonable in most cases to use Equation (1) as a maximum shear rate the fluid will encounter in blade coating.

For slot die coating, which is most common industrially, we can define a coating shear rate, as aforementioned, but also a wall shear rate

$$\dot{\gamma} = \frac{6Q}{bh^2} \quad (2)$$

where Q is the volumetric flow rate of material, b is the slot width, and h is the slot length. This shear rate is typically higher than the coating shear rate, but must be calculated specifically to the setup used to find the maximum shear rate encountered.

The viscosity at these shear rates can be directly extracted from steady shear rheology measurements. There is more information to be gained through oscillatory measurements, which allow the elastic and viscous contributions to be separated. However, it is more difficult to compare the oscillations, with a defined frequency and amplitude, to the steady shear flow in the coater. One way is using the Cox–Merz rule,^[19] which is the assumption that the complex viscosity at a given frequency is equal to the viscosity at a shear rate equal to that frequency.

Coating shear rates range from 500 to 10 000 s^{−1} between research draw down and industrial reel-to-reel coaters. Hence, while the lower end of this range (including the majority of slow research lab coating) can be reached in steady shear, in oscillation these high frequencies cannot be reached. This is usually because of the additional impact of inertia in oscillation, due to the frequent changes in direction of the motion.

For water-based anodes, using a CMC and SBR binder system, adsorption of binder onto the graphite has been shown to be key, producing electrostatic repulsion between particles which aids their dispersion.^[20] The binder concentration is also important, as the CMC can form an entangled polymer network, but at lower concentrations, the particle–particle interactions dictate the structure. Adsorption of CMC is impacted by its degree of substitution (DS), where lower DS allows more adsorption to graphite particles, and less free CMC, leading to a decrease in viscosity. Greater CMC adsorption to graphite has also been shown to increase adhesion to the current collector in the dried electrode.^[21]

PVDF–NMP is still a popular binder–solvent choice due to its chemical stability, and the good adhesive and cohesive properties of the coatings. The importance of the material processing to the final electrode properties is highlighted by an example of the method in which the carbon black and the active components are mixed or dispersed within the inks. LiNi_xMn_yCo_zO₂ (NMC) and LiFePO₄ (LFP) cathode materials show differences in dispersion depending upon the method of mixing.^[22] When the carbon black is dry mixed with the active components before dispersion, the carbon black was found to bind to the

surface of the NMC.^[23] This reduces the connectivity of the particles and hence the 3D-electronic conductivity of the final electrode coatings. When pre-dispersed in the NMP-PVDF, a 3D carbon network is formed connecting the components of the active materials.^[24] The dispersion of the carbon black is disrupted easily, and alternative binders such as PVP have shown to preferentially absorb the CB promoting agglomerations.^[25] This is reflected in the rheological properties of the inks, where for the dry mixing and poorly dispersed CB inks, only a weak gel is observed compared to the electrostatically stabilized network of carbon black formed with pre-dispersion which showed strong gel-like behaviors.^[26] The hydrodynamic forces of a PVDF-NMP graphite slurry have also been modelled. Here the molecular weight and concentration were linked to the colloidal attractive forces in the slurry, indicating how further optimization and control of the rheological properties can be achieved.^[27]

An important difference between water and NMP slurries is the behavior of carbon black, which is the opposite in the two solvents. In water, surfactant is required to form a stabilized dispersion of CB, whereas in NMP it forms a stabilized dispersion alone and surfactants actually destabilize the dispersion.^[28]

In addition to standard rheology. Large amplitude oscillatory shear (LAOS) results have been reported for electrode slurries. An increase in both G' and G'' is observed at high strains, but the origins of this effect have not been explored.^[22] Basch et al.^[29] observed this for very high-weight solids suspensions and theorized that it was caused by “contact forces” between carbon particles. There is an opportunity to study this behavior in more detail by decomposing the large amplitude oscillatory shear results using a Fourier transform.^[30]

There have also been attempts to correlate rheology with electrode performance, and important rheological properties have been identified. A high viscosity is required at low shear to prevent sedimentation as well as a low viscosity at higher shear rates to enable uniformity in the coating flow.^[31] However, it is difficult to draw any direct correlations between rheology and electrode performance, due to the variety of interdependent parameters in battery manufacture (e.g., formulations, mixing, coating, and drying processes). For example, for a slurry with low stability (high weight percent, large particles/agglomerates), increases in low shear viscosity will prevent sedimentation, but for a highly stable slurry, this may provide no benefit, and the formulation changes made to achieve this (e.g., the addition of more binder) may lead to increases in the high shear viscosity as well, which impacts the coating flow negatively. Hence there is no one ‘universal’ rheology that needs to be achieved—the ideal rheology will be a function of the slurry structure, the coating process, and potentially the subsequent drying, calendaring, and assembly steps (e.g., high viscosities may inhibit drying, or a more elastic slurry rheology may give a more flexible coating that is easier to calendar and assemble).

Rheology is dependent on so many variables in the manufacturing process, and even at the slurry stage, there is a huge possible variation in formulation and mixing parameters. Hence, it is vital to have data for real industrial systems, as well as an in-depth understanding of how the interactions involved combining to give the resulting rheological behavior. Here, we advance this understanding by providing a systematic characterization of the rheological properties of anode and cathode

slurries. We use industrially relevant formulations and weight percentages (with high weight percentages (50–60%) and optimized levels of conductive additive and), as much current research is based on easier to process research formulations (e.g., weight percentages 20%–40%, excess of conductive additive and binder). A full factorial of possible components and combinations is performed, measuring steady shear, small, and large amplitude oscillatory shear properties, including Fourier transform rheology to probe the LAOS response.

2. Experimental Section

2.1. Materials and Mixing

Cathode slurries 96%w/w NMC, 2% PVDF, and 2% CB, at 60% weight solids in NMP, were made by pre-dissolving PVDF (Solvay SOLEF5130) in NMP (Honeywell M79603) for 5 hrs using a Silverson overhead mixer. Carbon black (C65 Imerys) was dispersed using an Intertronics Thinky mixer, for 1 min at 500 rpm, and 5 min at 2000 rpm. NMC622 (BASF) was added and dispersed similarly followed by a degas step of 2200 rpm for 3 min.

Anode slurries of 95.25%w/w graphite, 1.5% CMC, 2.25% SBR and 1% CB in water at a weight solids of 49.5%. were made in an analogous manner; carbon-black (C45, Imerys) was pre-dispersed in the CMC (Ashland BVH8) to which graphite (BTR S360 E3) was added using the same mixing protocols as for the NMC. A secondary binder, Zeon BM451-B SBR, was added at the end of the mix and dispersed at 500 rpm for 5 min.

Where the components and all possible material combinations were made for testing, they were prepared individually but followed the full outlined mixing procedure to ensure the mixes had all received the same treatment. Components were studied individually, maintaining the ratios of components to each other (when present) and solvent. To calculate the effective weight fraction required, the mass of the component in the final slurry was divided by the mass of solvent and any other components to be added.

For example, for 100 g of anode slurry, there is $100\text{ g} \times 95.25\% \times 49.5\% = 47.15\text{ g}$ of Graphite in the slurry, and 50.5 g of water, so to study graphite alone, the weight percentage required is $47.15/(50.5 + 47.15) \times 100 = 48.3\%$. When SBR is included, per 100 g of slurry there is then still 47.15 g of graphite, but now also $100\text{ g} \times 2.25\% \times 49.5\% = 1.11\text{ g}$ of SBR. The weight percentage of graphite then becomes $47.15/(50.5 + 47.15 + 1.11) \times 100 = 47.8\%$ and the weight percentage of SBR: $1.11/(50.5 + 47.15 + 1.11) = 1.12\%$.

This was done for all components so the ratio of components to water was fixed, and the same as in the final slurry. The full ratios for all components are given in **Table 1**.

2.2. Microscopy

A drop of solution/slurry was applied to a glass slide and imaged with a 20× lens using a Leica microscope in focus variation mode. The lens was moved up and down and limits where no sample was in focus were found at each end, then a scan was performed between these two limits.

Table 1. Anode and cathode formulations used in this study.

Cathode Formulation (solids)	96% NMC, 2% PVDF and 2% CB				
Weight percentage in NMP	60%				
	Percentage in Slurry (by mass)				
	NMC	PVDF	CB	NMP	
CB	0.00	0.00	2.91	97.09	
CB + NMC	58.24	0.00	1.21	40.55	
CB + PVDF	0.00	2.83	2.83	94.34	
CB + NMC + PVDF	57.61	1.20	1.20	39.99	
NMC	58.95	0.00	0.00	41.05	
NMC + PVDF	58.31	1.21	0.00	40.48	
PVDF	0.00	2.91	0.00	97.09	
Anode Formulation (solids)	95.25% Graphite, 1.5% CMC, 2.25% SBR and 1% CB				
Weight percentage in water	50%				
	Percentage in Slurry (by mass)				
	GRA	CMC	SBR	CB	Water
GRA	48.30	0.00	0.00	0.00	51.70
GRA + CB + CMC	47.70	0.75	0.00	0.50	51.05
CB + CMC + SBR	0.00	1.40	2.11	0.94	95.55
CB	0.00	0.00	0.00	0.98	99.02
CB + SBR	0.00	0.00	2.14	0.95	96.91
CMC + CB	0.00	1.44	0.00	0.96	97.60
GRA + CB + CMC + SBR	47.18	0.74	1.11	0.50	50.47
CMC + SBR	0.00	1.42	2.12	0.00	96.46
GRA + CB	48.10	0.00	0.00	0.50	51.40
GRA + CMC + SBR	47.42	0.75	1.12	0.00	50.71
SBR	0.00	0.00	2.13	0.00	97.87
CMC	0.00	1.42	0.00	0.00	98.58
GRA + CMC	47.96	0.76	0.00	0.00	51.28
GRA + SBR	47.80	0.00	1.12	0.00	51.08
GRA + CB + SBR	47.53	0.00	1.13	0.50	50.84

2.3. Rheological Measurements

Rheology was measured using a Netzsch Kinexus Pro+ rheometer equipped with a 40 mm roughened parallel plate, a roughened lower plate, and a measuring gap of 1 mm. Samples were loaded, and the gap was set to 1.05 mm. Samples were then trimmed, and the gap lowered to 1 mm to ensure there was no underfilling.

The temperature was maintained at 25 °C using a Peltier plate and enclosure. A constant temperature was chosen, because while the temperature is an important variable for the rheology, there is a narrow range of temperatures that these slurries can be processed at to avoid freezing, or rapid drying of the slurry. Because of this small operating range, time–temperature superposition,^[32,33] which is commonly used to provide wider frequency ranges in oscillatory rheology, provides little benefit here, and may be difficult to interpret due to the complexity of the slurries, so was not applied.

Flow curves were performed between 0.1 and 1000 s^{−1} and equilibrium was deemed to be reached when the measured value

was within 1% for 10 s. Amplitude sweeps were performed between 0.01% and 1000% at 1 Hz. Frequency sweeps were then performed at a strain in the Linear Viscoelastic Region for each sample (between 0.015% and 10%, see Figure captions for values), for a frequency range between 0.1 and 628 Hz. The range of some sweeps is smaller as the sample started to leave the gap at which point the test was stopped. The amplitude sweep results were analyzed by Fourier transform rheology using in-house software.^[34]

3. Results and Discussion

3.1. Anode Slurries

3.1.1. Steady Shear Rheology

The rheology of a typical industrial water-based anode slurry, consisting of graphite, carbon black, CMC, and SBR binders was characterized by steady shear. The flow curves of this anode, and all combinations of the components in water, are shown in **Figure 1**. A model is fit to the data to extract key parameters for comparison. The chosen model was developed for high solids loading nuclear waste slurries,^[35] and consists of a cross model for shear-thinning fluids, plus a yield stress

$$\eta(\dot{\gamma}) = \eta_{\infty} + \frac{\eta_0 - \eta_{\infty}}{1 + (\tau\dot{\gamma})^m} + \frac{\sigma_y}{\dot{\gamma}} \quad (3)$$

where $\eta(\dot{\gamma})$ is the viscosity at shear rate, $\dot{\gamma}$, η_{∞} is the viscosity at infinite shear rate, η_0 is the zero shear viscosity, τ is the cross-time constant, m is the cross-consistency factor, and σ_y is the yield stress. This model, fit via a difference of least squares procedure, allowed all components to be represented and the parameters then highlight which components displayed yield stress behavior, zero shear viscosities, and infinite viscosity behavior. The model parameters are given in **Table 2**.

As well as capturing the wide range of the behavior of the different components, the model also provides better fits to the final slurry. The shape of the anode slurry graph indicates shear thinning with a zero-shear viscosity, which can be captured with a cross model, however, at low shear rates, there is a slight increase in viscosity which is additionally captured when yield stress is added, and may have been missed without comparing the model with and without a yield stress.

In the components, we can identify two types of behavior. All the particulate materials without CMC binder (CB, GRA, CB + GRA, CB + GRA + SBR, CB + SBR, GRA + SBR), show steep decreases in the viscosity with shear rate, which is likely due to agglomeration, and the agglomerates breaking up with increased shear. For example, cement, a dense particulate suspension, also shows steep shear thinning without added dispersants, which is attributed to the breakup of flocculated material under shear.^[36] The viscosity values increase as more components are added, as they are all hydrophobic, and so produce increased agglomeration when combined in large amounts. They also notably show noise in the results, with jumps likely indicating some slip in the measurement, despite the roughened geometries. There is consequentially also a more significant error in the fits, shown

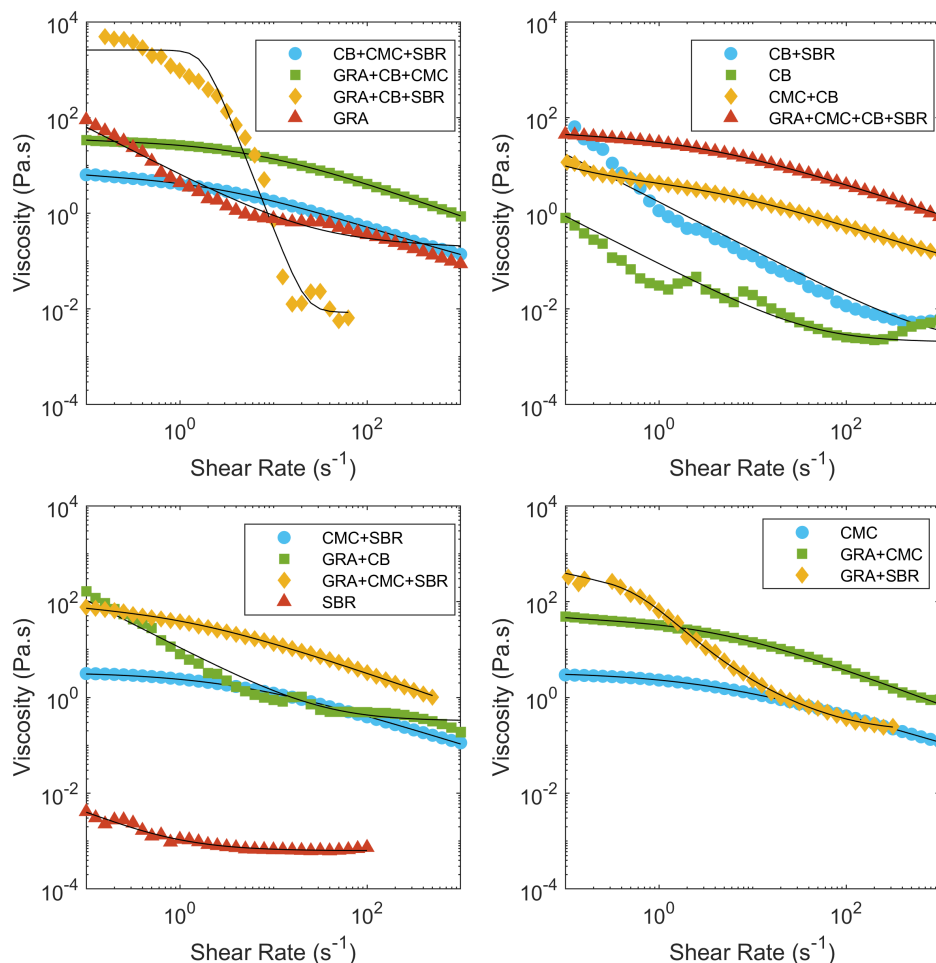


Figure 1. Flow curves of all components of an industrial anode slurry, black lines indicate fits with the cross model with a yield stress.

by the higher least squares difference. Without the CMC these particle dispersions are not stable, while they did not settle out visibly over the course of the measurement, under the microscope, large agglomerates of CB formed in water (see **Figure 2**). This instability means they are more likely to show artifacts in the steady shear rheology.

All the CMC-containing mixtures have a very similar shape to their rheology, a zero-shear viscosity followed by shear thinning, which is clearly dictated by the behavior of the CMC polymer. The CMC is the only component that dissolves in the solvent (water) and creates a thickened solution in which the other components can be more easily suspended.

Within the CMC-containing mixtures, two groups can be seen, where the mixtures including Graphite are shifted to ≈ 10 times higher viscosity, (shown by ≈ 10 times increase in η_0) likely due to the large volume of particles added.

This can be compared to equations for the viscosity increase on the addition of particles to a solution. For example, the Krieger–Dougherty equation^[37]

$$\eta = \eta_0 \left(1 - \frac{\phi}{\phi_{\max}} \right)^{-[\eta]\phi_{\max}} \quad (4)$$

where η_0 is the viscosity of the matrix alone, ϕ is the volume fraction, and ϕ_{\max} is the maximum volume fraction at which the mixture will still flow, for spheres the maximum packing can be used which is in the range 0.52–0.74.^[38]

The value of the intrinsic viscosity can be calculated using the following equation^[39,40] for nonspherical particles

$$[\eta] = 2.5 + 0.123(R - 1)^{0.925} \quad (5)$$

where $[\eta]$ is the intrinsic viscosity, R is the aspect ratio of the particles, e.g., a value of 2 indicates the particles are 2 times as long as they are wide.

BTR graphite is a disperse mixture of smaller and larger particles, which likely impacts the maximum packing fraction as the two sizes of the particles will pack much better than one size alone. The aspect ratio of the larger fraction is around 2 from the manufacturer's specifications.

Using $\eta/\eta_0 = 10$ for the addition of graphite, as observed in the rheology, then using the solid volume fraction of graphite added of 0.295, this implies the slurry is very close to the maximum packing fraction which is calculated as 0.314.

Using the current mixing procedure, mixes of 0.32 volume fraction graphite were not possible, forming large clumps of

Table 2. Fitting parameters for anode slurry components with the cross+yield model.

Sample	Infinite Viscosity η_{∞} [Pa s]	Zero Shear Viscosity η_0 [Pa s]	Cross-time Constant τ [s]	Yield Stress σ_y [Pa]	Cross-consistency Factor [m]	Least Squares Difference (Error)
GRA	0.0000	0.7982	0.0975	6.2701	67.8331	4.4956
GRA + CB + CMC	0.0000	33.3819	0.7028	0.2158	0.1699	0.0035
CB + CMC + SBR	0.0238	6.4662	0.6590	0.0563	0.4463	0.0166
CB	0.0020	0.0020	0.0000	0.0870	0.0009	16.5070
CB + SBR	0.0019	0.0075	3.3948	1.7170	0.6238	23.1490
CMC + CB	0.0227	5.3404	0.6654	0.4815	0.2915	0.0025
GRA + CB + CMC + SBR	0.0000	47.0182	0.6422	0.2794	0.4253	0.0138
CMC + SBR	0.0009	3.3941	0.6213	0.0000	0.2543	0.0333
GRA + CB	0.0000	0.6457	0.0000	10.6517	47.4928	4.9670
GRA + CMC + SBR	0.0000	80.9793	0.6751	0.6816	1.1522	0.1187
SBR	0.0006	0.0308	0.9306	0.0000	92.4811	0.3191
CMC	0.0003	3.3850	0.5928	0.0000	0.2808	0.0015
GRA + CMC	0.0000	44.1321	0.7314	0.4976	0.2722	0.0699
GRA + SBR	0.1885	234.7578	2.0981	16.2240	1.8641	0.1714
GRA + CB + SBR	0.0084	2576.2651	4.9974	0.0000	0.5570	17.6997

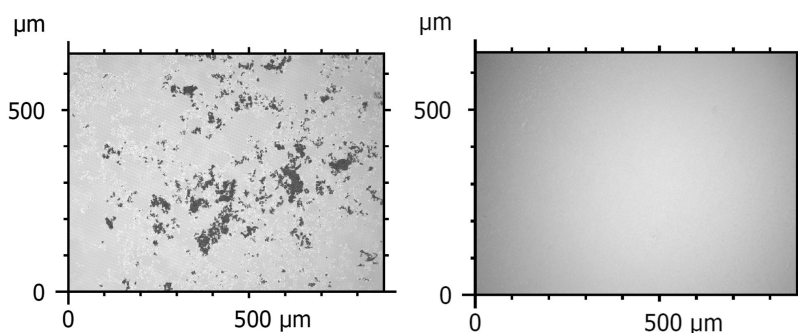


Figure 2. Optical microscopy at 20 \times of the surface of a drop of C45 in water versus C65 in N-methyl pyrrolidone (NMP), showing that the water-based carbon black is agglomerated but agglomerates cannot be seen at this resolution for the NMP-based formulation.

the unmixed powder, suggesting that the Krieger–Dougherty equation has correctly predicted the maximum fraction of agglomerates. This implies that the viscosity increase is due to the addition of particles and that there are no additional interactions between the graphite and other slurry components.

However, with more intensive mixing a slurry could be formed at this weight fraction (additional stirring and Thinky mixing steps). This is likely due to the size of the agglomerates being dependent on the mixing procedure, which would affect the parameters in the equations given earlier. This has been previously reported, with rheology changes as the mixing procedure is changed (more intensive mixing gives smaller agglomerates which causes a reduction in the viscosity).^[6]

The proximity to the maximum packing fraction suggests the formulation meets the industrial requirement of reducing solvent (in turn reducing drying times and energy required). It also highlights the need for characterization at these industrial weight fractions, as the rheology in this region will be very different from more dilute dispersions, commonly encountered in research.

3.1.2. Oscillatory

Frequency Sweeps: The frequency sweeps (**Figure 3**) show that the mixes without CMC, as well as having high viscosity, display elastic behavior ($G' > G''$), which is likely due to the formation of large solid agglomerates. The difference between G' and G'' increases with the viscosity and the addition of SBR causes a dramatic increase in both, suggesting again that the SBR promotes this agglomeration. The CMC is required to create a flowing mixture ($G'' > G'$) which will coat without instability. The majority of mixes including CMC show similar behavior, again suggesting it dictates the rheology of these water-based anodes.

This data can also be used in optimization, as slurries with G' much greater than G'' will likely have instabilities in flow during coating, forming nonuniform coatings. This can be used to find the maximum weight solids that will still flow, thus reducing the solvent required and energy required during drying. This industrial slurry is close to this limit, being close to the maximum packing fraction and thus having G' close to G'' .

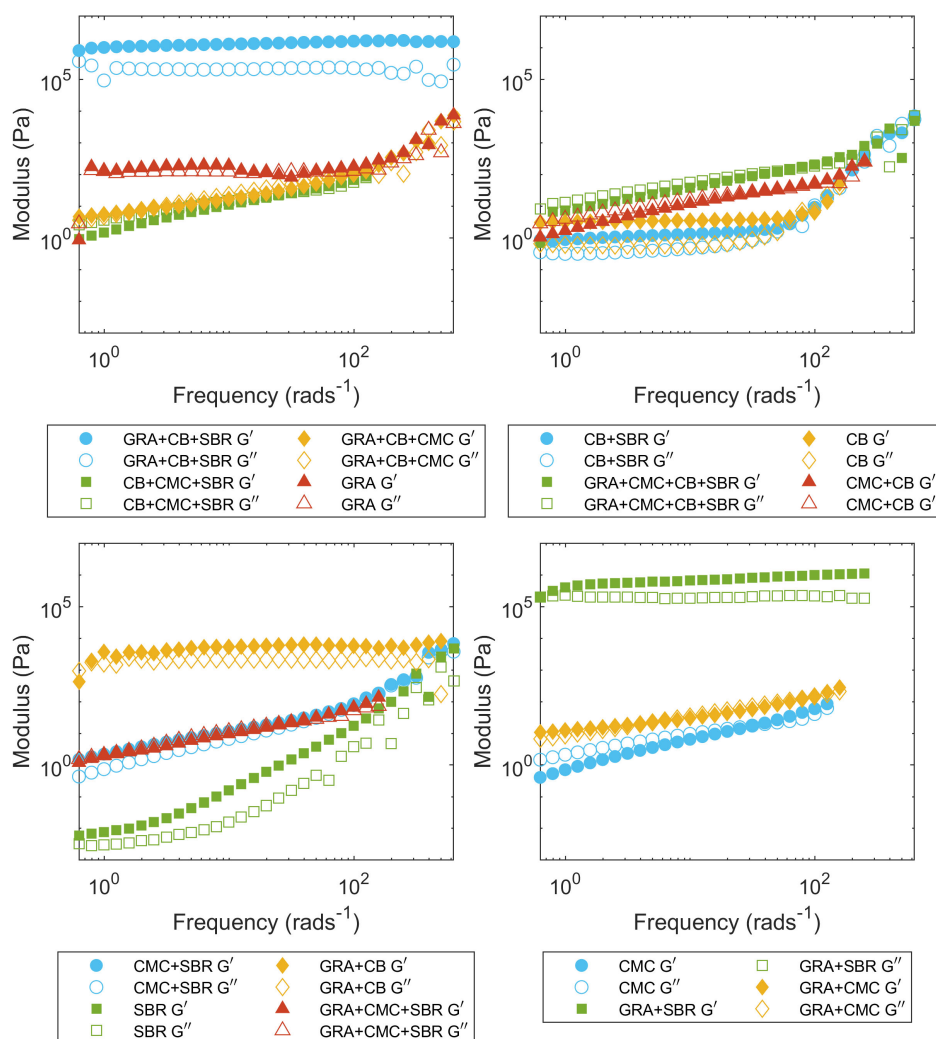


Figure 3. Anode oscillatory frequency sweeps measured at a strain keep sample in the LVE): GRA + SBR: 0.015% GRA + CB + SBR: 0.075%, GRA + CMC + CB + SBR, GRA + CB: 0.1%, CMC, GRA + CMC, CMC + SBR, CB + CMC + SBR, GRA, GRA + CB + CMC, GRA + CMC + SBR: 0.5%, CMC + CB: 5%, CB, CB + SBR, SBR: 10%.

Amplitude Sweeps and LAOS: The amplitude sweeps (Figure 4) show a similar picture, however, there is one key difference, some of the mixtures show a bump in both moduli at high strain. This is not seen for CMC alone and thus not a characteristic of the polymer matrix, unlike many of the other rheological properties. This is only seen when particles are incorporated with the CMC, and could potentially be a particle jamming event, when the suspended particles begin to collide. This is overcome at higher strain but may have implications for coating, e.g., higher pressures required to overcome this resistance.

These sweeps were further analyzed by Fourier transform rheology (Figure 5). The “bump” in linear moduli is accompanied by a peak in G_3'' and a negative peak in G_3' . Using the definitions proposed by Ewoldt et al.^[41] we can interpret these parameters as follows.

G_3' {+: strain softening, – strain hardening

G_3'' {+: shear thickening, – shear thinning

Thus, this implies strain hardening and shear thickening for the anode slurries, which would be the case for a particle jamming event.^[42] However, it is interesting that this is overcome, i.e., the behavior is a “bump” in the moduli rather than a continuous increase. This could suggest that the jamming induces the breakup of agglomerates that allow the bulk slurry to flow again.

It is clear from the rheology that the water-based graphite ink is stabilized by the thickening agent CMC. The rheology arising from the CMC-in water dominates the rheological response of the total slurry, with the viscosity of the mix increasing with the addition of the large graphite solid content. CMC is ideal for this role, having a strongly shear thinning response, giving high viscosity at low shear to stabilize the slurry, but shear thinning rapidly to allow flow in the coater. SBR is purely a binder for flexibility and adhesion properties in the dry coating, as there is very little rheological response with the addition of SBR to the slurry. However, without CMC, the SBR promotes agglomeration of both the carbon black and the graphite in

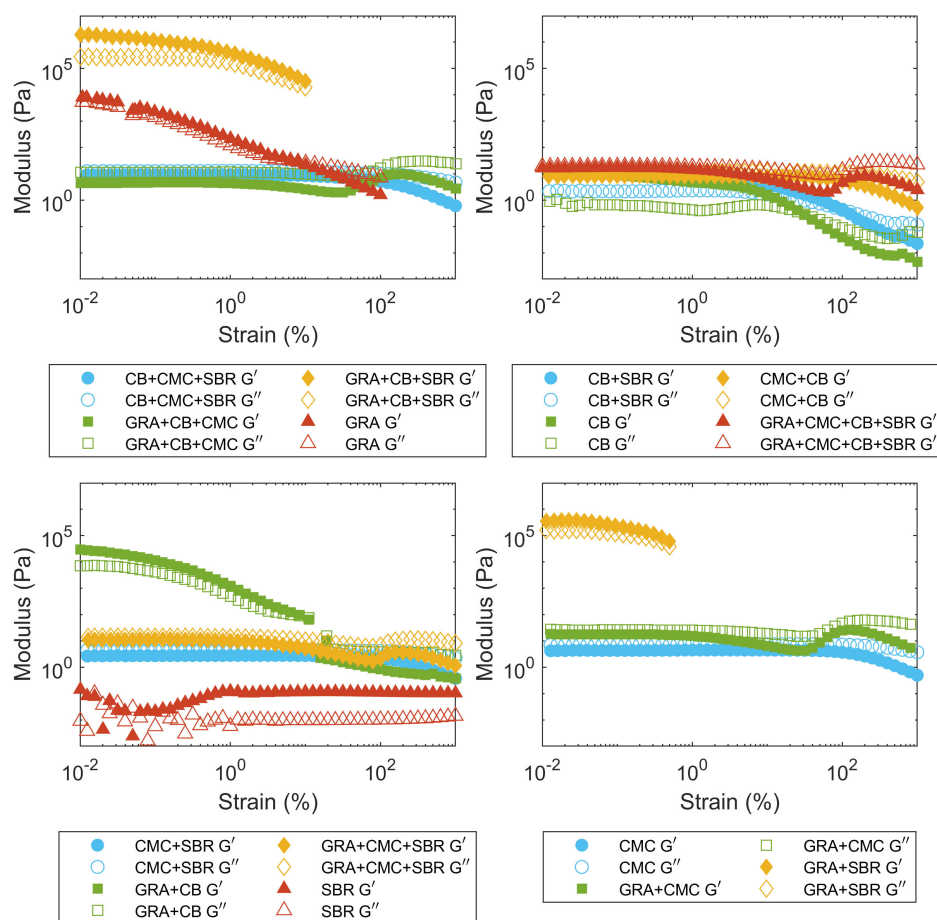


Figure 4. Anode amplitude sweeps measured at 6.23 rad s^{-1} .

the mix, and reduction of SBR content may aid stability in novel formulations.

However, the behavior of CB in water is nonideal, it is agglomerates which makes it difficult to form a conductive network. In the mixing procedure, CB is premixed with CMC before graphite is added. It appears that this is effective in dispersing the CB, which gives an increase in viscosity and the onset of a yield stress over the CMC alone, as well as moving suggesting a particle network has formed. The viscosity at low shear rates (or a fit to extract the yield stress) could be a key measure to measure the efficiency of this mixing step and thus the ability to form a conductive network in the final slurry.

3.2. Cathode Slurries

3.2.1. Steady Shear Rheology

The cathode slurries consisted of NMC622 in NMP with carbon black additive and PVDF binder. Their behavior was significantly different from the anode, as can be seen in the flow curves in **Figure 6**, with fitting parameters in **Table 3**. We can see the carbon black has very high initial viscosity alone, again it shear thins, but observing the solution under the microscope suggests

the carbon black is not agglomerated (**Figure 2**). The mixes without carbon black have a significantly lower viscosity at low shear rates than those containing CB, with 1 outlier, CB + NMC, which has a very low viscosity, slightly higher than NMC alone at low and high shear rates, but very close to the NMC in the intermediate region.

The behavior could be explained by the formation of a CB network in NMP, which can be broken by shear but is much more stable than the agglomerates formed in water. When NMC is added, the majority of the CB adsorbs to the surface of the NMC, meaning there is little free CB to form this network and give the increased viscosity. However, when PVDF is added, it preferentially adsorbs to the NMC particles, displacing CB, meaning more free CB is available in the solvent.

It has been reported in the literature that carbon black forms stable suspensions in NMC but not in water, and that the behavior in some tests is opposite in the two tests. This is attributed to the better match of NMP to the hydrophobicity of carbon black. Carbon is hydrophobic, but charges on the surface of particles mean it is not stable in nonpolar solvents, and thus can only be stabilized in intermediate polarity solvents such as NMP.^[22]

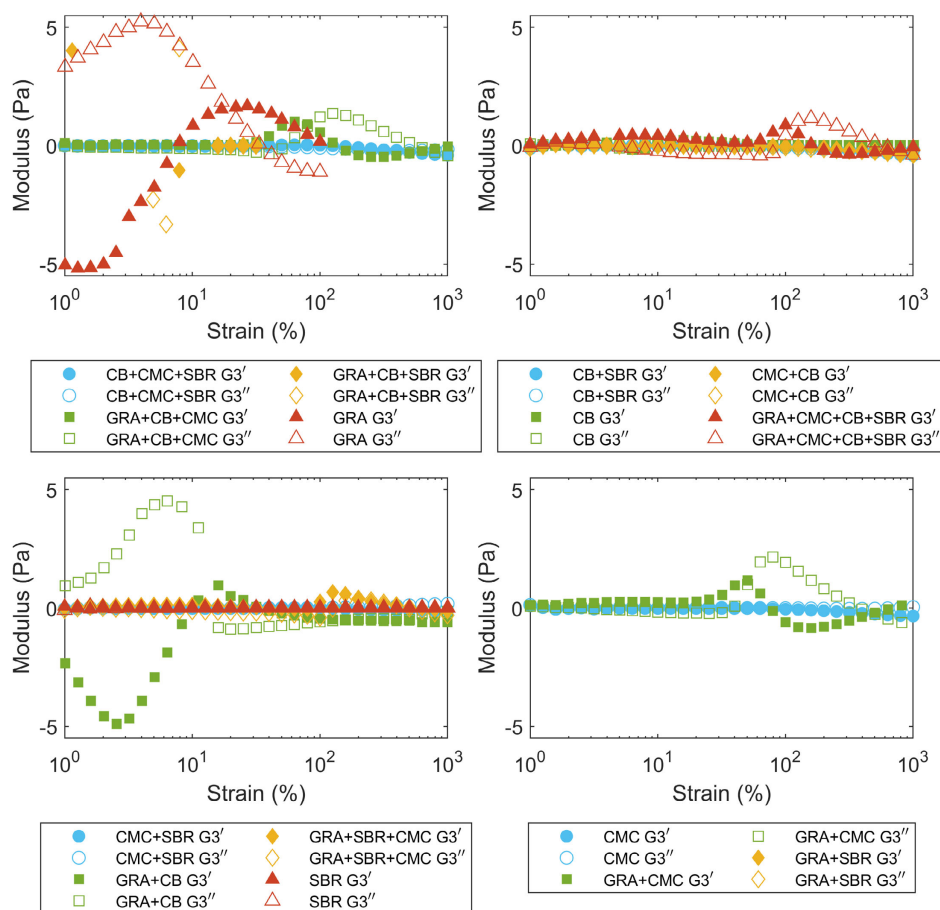


Figure 5. Third harmonic parameters from anode amplitude sweeps measured at 6.23 rad s^{-1} .

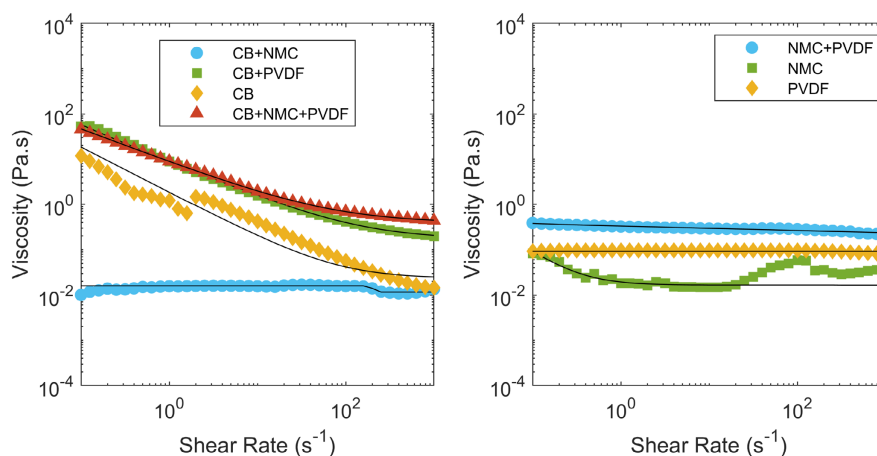


Figure 6. Flow curves of all components of an industrial cathode slurry.

3.2.2. Oscillatory Rheology

Frequency Sweeps: Interestingly, for the majority of frequencies observed, the carbon black and carbon black with PVDF, show elastic behavior, suggesting a stable network of the carbon black

(Figure 7). However, when the NMC is added, the behavior is much more viscoelastic ($G' \approx G''$), which could be explained by a reduction in the amount of free CB by adsorption to the added NMC particles. Further evidence for this is seen in the CB + NMC curve, which would be expected to have less free

Table 3. Fitting parameters for cathode slurry components with the cross+yield model.

Sample	Infinite Viscosity η_{∞} [Pa s]	Zero Shear Viscosity η_0 [Pa s]	Cross-time Constant τ [s]	Yield Stress σ_y [Pa]	Cross-consistency Factor [m]	Least Squares Difference (Error)
CB	0.0231	0.0000	68.5699	1.8563	0.5575	13.9769
CB + NMC	0.0116	0.0159	68.6154	0.0000	0.0050	0.0559
CB + PVDF	0.1698	15.7636	0.7415	4.7564	3.9783	0.8012
CB + NMC + PVDF	0.3900	490.8001	0.7100	0.9581	345.0756	0.0448
NMC	0.0165	0.7699	1.4704	0.0000	44.7812	0.9173
NMC + PVDF	0.0773	0.7026	0.1000	0.0014	42.8532	0.0664
PVDF	0.0000	0.0925	1.0000	0.0000	0.0000	0.0688

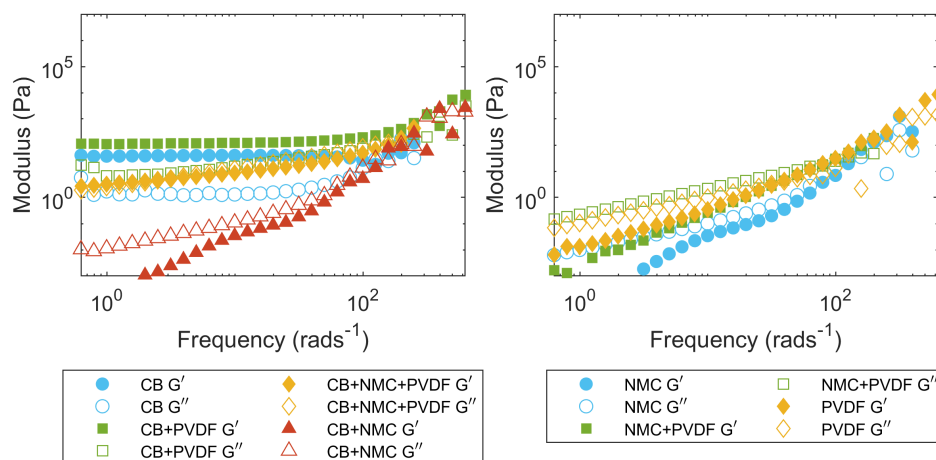


Figure 7. Cathode oscillatory frequency sweeps measured at strains to keep sample in the LVE: CB: 0.1%, CB + PVDF: 0.2%, GRA + CMC + CB + SBR: 0.5%, NMC + PVDF, PVDF: 2%, CB + NMC, NMC:10%.

CB (as PVDF will displace some of CB from the NMC particles when present) and shows much more viscous behavior ($G' < G''$). Carbon black is known to accumulate on the surface of NMC particles and this approach has been used to protect higher nickel content NMCs from side reactions,^[43] but can also be undesirable as it makes forming a conducting network more difficult.

Hence there is a balance between allowing enough free carbon black in the solution to form a network (this will advantageously increase the viscosity allowing better suspension of the NMC, and give a network of CB in the final electrode, which is key to good conductivity, particularly for NMC as it has a low conductivity itself), and not having so much CB that the rheology becomes gel-like, which could result in instabilities in the coater and uneven coatings. Therefore, these frequency sweeps are also a useful tool for optimization of the NMP-based cathode slurries.

Amplitude Sweeps and LAOS: In the amplitude sweeps (Figure 8), we can see again that the behavior of the final slurry is an intermediate between the carbon black, and the remaining components. Again CB + NMC is an outlier, having similar behavior to NMC alone, but for the other mixes with CB present, breakdown of the network is seen at higher strains, most dramatically for the CB alone and CB and PVDF.

The amplitude sweeps were also analyzed by Fourier transform rheology to extract G_3' and G_3'' (Figure 9). A similar but much smaller “bump” in the linear moduli is observed for the cathode mixtures. However, it is accompanied by a negative peak in G_3'' and a positive peak in G_3' , opposite to the anode slurries. This combination of shear and strain thinning could suggest a network breakdown, and the effect could be caused by the breaking of the carbon black-NMP network formed, causing a lag in the linear moduli as additional energy is required to overcome these interactions.

The NMP-based cathode displays very different behavior to the water-based anode. For this system, the dispersion of carbon black is simpler, as it forms a network alone in NMP. However, it will adsorb preferentially to the N1610

1610MC particles when they are included, so the function of the binder is not only to thicken the solvent to allow suspension of the particles, but also to occupy the surface of the NMC particles to displace the CB and allow it to form a conducting network. The coating of the active material particles in polymeric binder could be the reason PVDF systems have better adhesion and flexibility than water-based anodes (which require additional SBR for these properties). This leads to suggestions for water-based processing, where milling or

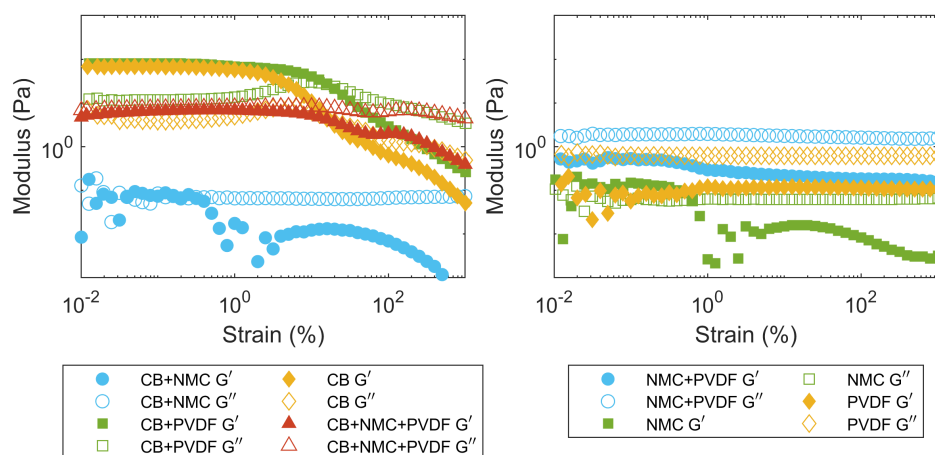


Figure 8. Cathode amplitude sweeps measured at 6.23 rad^{-1} .

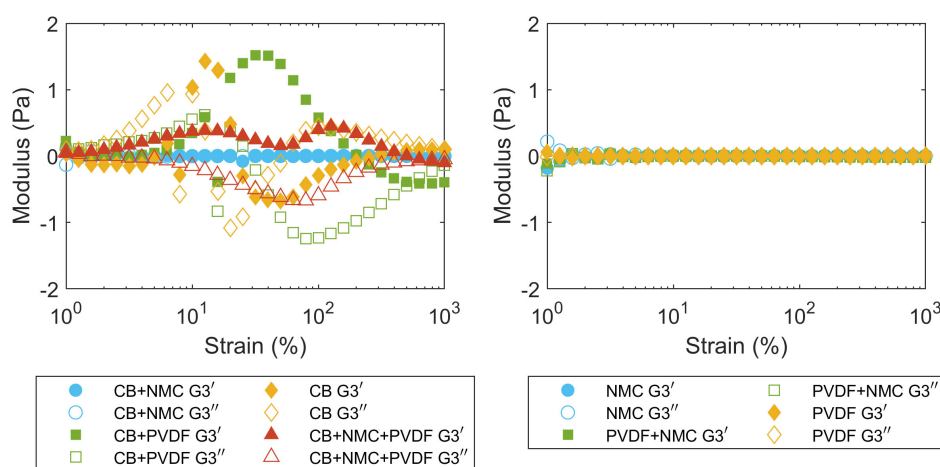


Figure 9. Third harmonic parameters from Cathode amplitude sweeps measured at 6.23 rad^{-1} .

premixing the active material with a binder may enhance adhesion. An illustration of the structures in water and NMP solvents is given in **Figure 10**.

This has key implications for replacing PVDF as a binder, as any binder must not also thicken the slurry, but also adsorb to the surface of the active material, to displace CB. Without this function, excessive carbon black would be required and thus less active material, lowering the energy density of the final coating. It could also provide insights into the mixing process, where milling or premixing the active material with the binder may aid this function.

It is also important to consider this function when attempting to move to water-based processing for cathodes, especially as NMC has a much lower conductivity than graphite, so forming the conductive network with an additive is key to the final electronic properties. The PVDF clearly plays a very different role in the rheology to the CMC in water, as it gives a much smaller viscosity alone than in the final slurry, and shows Newtonian behavior, unlike the full slurry.

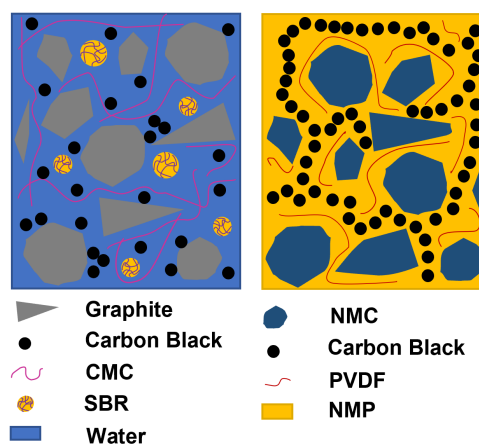


Figure 10. Illustration of structure in anode (left) and cathode (right) slurries, showing the polymer network dominant in water where the carbon black network is dominant in NMP.

4. Conclusions

The impact of components used in both anode and cathode slurries on the final slurry rheology has been assessed, and the slurry rheology is used to infer a microstructure within the slurry. With this knowledge, recommendations are made for rheological optimization. 1) The rheology different for industrially relevant inks, both anodes and cathodes have been characterized, at relevant weight percentages (49.5% anodes, 60% cathodes) 2) The rheology of industrially relevant inks, both an anode (49.5 wt%) and cathode (60 wt%) have been characterized, while both exhibit shear thinning behavior, their rheology differs significantly: i) Anode slurries demonstrate shear thinning behavior with a zero-shear viscosity ii) Cathodes demonstrate weakly gel-like behavior, with a yield stress followed by thinning until an infinite viscosity is reached. 3) The contributions of different components to the rheology is clear: i) In water-based anodes the CMC dictates the rheology, creating a thickened matrix in which the graphite, carbon black and SBR are suspended. As the packing fraction of graphite is close to the maximum, without CMC, the other components agglomerate, creating highly unstable solid-like slurries. With CMC, the addition of CB and SBR has little impact on the rheology, and graphite only increases the viscosity as would be expected for the amount of particles added in suspension. ii) In NMP-based cathodes, the carbon black network dictates the rheology, and the rheology of CB alone is similar to that of the final slurry. The addition of NMC provides a surface that the CB can adsorb to, removing it from the solution and breaking this network, and making the rheology again resemble the solvent alone. However, when the PVDF binder is present, it preferentially adsorbs to NMC, freeing the CB again to return the network and the rheological properties. 4) LAOS behavior is studied and G_3' and G_3'' are extracted using a Fourier transform. "Bumps" are observed in the LAOS behavior, for anodes this is typical of particle jamming, but is overcome, possibly by the breakup of agglomerates after the jam. Cathodes also show this behavior but there is an equal magnitude of both shear and strain thinning, suggesting a breakdown of the CB network. 5) These results also have implications for the optimization of slurry rheology. To tune anode rheology, the CMC binder should be the focus, adapting concentration, molecular weight, and degree of substitution (DS) to achieve the required properties. Whereas for cathodes, the rheology is dependent on the amount of free CB, which is a delicate balance between the amount of CB available to form a space-spanning network (can be tuned by changing amount of CB added, or mixing to break up CB agglomerates) and the amount of free NMC surface the CB can adsorb to (can be tuned by the amount of NMC, and the adsorption properties of the binder, which displaces CB from the surface). 6) There are also implications for novel formulations and improving sustainability: i) To replace SBR in water-based systems, a replacement binder must adhere strongly to the particle interfaces (which could be promoted by premixing or milling) to enhance adhesion. ii) To replace PVDF, a binder is required which similarly occupies the active material interfaces and allows free carbon black to form a network in solution to give the required rheology and conductivity of the final electrode. iii) If moving to water-based cathodes, as well as a binder to occupy active material interfaces, the enhanced focus will need to be

given to overcoming agglomeration of the carbon black (e.g., through dispersants), to achieve the required electronic properties. 7) These results provide useful insights for optimizing industrial slurries and highlight the role rheology can play in formulation optimization. While the majority of insights also apply to more dilute formulations, close to the formulation limits, rheology changes rapidly, and thus the results provide useful comparisons for predicting how research formulations may behave when weight solids are increased.

Acknowledgements

This work was supported by the Faraday Institution NEXTRIDE project (faraday.ac.uk; EP/S003053/1, FIRG015).

Conflict of Interest

The authors declare no conflict of interest.

Data Availability Statement

The data that support the findings of this study are available from the corresponding author upon reasonable request.

Keywords

anodes, battery manufacturing, cathodes, rheology, slurries, structures

Received: May 24, 2022

Revised: July 30, 2022

Published online: September 6, 2022

- [1] E. Kendrick, *Future Lithium-Ion Batteries*, chapter 11, RSC, Cambridge **2019**, pp. 262–289.
- [2] C. D. Reynolds, P. R. Slater, S. D. Hare, M. J. H. Simmons, E. Kendrick, *Mater. Des.* **2021**, 209, 109971.
- [3] Y. S. Zhang, N. E. Courtier, Z. Zhang, K. Liu, J. J. Bailey, A. M. Boyce, G. Richardson, P. R. Shearing, E. Kendrick, D. J. L. Brett, *Adv. Energy Mater.* **2022**, 12, 2102233.
- [4] K. Wang, Y. Wu, S. Luo, X. He, J. Wang, K. Jiang, S. Fan, *J. Power Sources* **2013**, 233, 209.
- [5] Y. Shi, L. Wen, S. Pei, M. Wu, F. Li, *J. Energy Chem.* **2019**, 30, 19.
- [6] H. Bockholt, W. Haselrieder, A. Kwade, *ECS Trans.* **2013**, 50, 25.
- [7] D. Bresser, D. Buchholz, A. Moretti, A. Varzi, S. Passerini, *Energy Environ. Sci.* **2018**, 11, 3096.
- [8] J. E. Marshall, A. Zhenova, S. Roberts, T. Petchey, P. Zhu, C. E. J. Dancer, C. R. McElroy, E. Kendrick, V. Goodship, *Polymers* **2021**, 13, 1354.
- [9] Y. He, L. Jing, Y. Ji, Z. Zhu, L. Feng, X. Fu, Y. Wang, *J. Energy Chem.* **2022**, 72, 41.
- [10] D. Gastol, M. Capener, C. Reynolds, C. Constable, E. Kendrick, *Mater. Des.* **2021**, 205, 109720.
- [11] Y. S. Zhang, J. J. Bailey, Y. Sun, A. M. Boyce, W. Dawson, C. D. Reynolds, Z. Zhang, X. Lu, P. Grant, E. Kendrick, P. R. Shearing, D. J. L. Brett, *J. Mater. Chem. A* **2022**, 10, 10593.
- [12] L. Jing, Y. Ji, L. Feng, X. Fu, X. He, Y. He, Z. Zhu, X. Sun, Z. Liu, M. Yang, W. Yang, Y. Wang, *Energy Storage Mater.* **2022**, 45, 828.
- [13] L. Feng, Y. Ji, Z. Zhu, P. Yu, X. Fu, M. Yang, Y. Wang, W. Yang, *Energy Storage Mater.* **2021**, 40, 415.

- [14] S. X. Drakopoulos, A. Gholamipour-Shirazi, P. MacDonald, R. C. Parini, C. D. Reynolds, D. L. Burnett, B. Pye, K. B. O'Regan, G. Wang, T. M. Whitehead, G. J. Conduit, A. Cazacu, E. Kendrick, *Cell Reports Phys. Sci.* **2021**, 2, 100683.
- [15] S. Shi, J. Gao, Y. Liu, Y. Zhao, Q. Wu, W. Ju, C. Ouyang, R. Xiao, *Chinese Phys. B.* **2015**, 25, 018212.
- [16] E. Kendrick, M. Faraji, C. Reynolds, L. Aa, J. Marco, *Energy Storage Mater.* **2022**, 51, 223.
- [17] T. G. Mezger, *The Rheology Handbook*, 4th ed., Vincentz Network **2012**.
- [18] M. Maillard, C. Mézière, P. Moucheron, C. Courrier, P. Coussot, *J. Non-Newton. Fluid Mech.* **2016**, 237, 16.
- [19] W. P. Cox, E. H. Merz, *J. Polym. Sci.* **1958**, 28, 619.
- [20] S. Lim, S. Kim, K. H. Ahn, S. J. Lee, *J. Power Sources* **2015**, 299, 221.
- [21] J.-H. Lee, U. Paik, V. A. Hackley, Y.-M. Choi, *J. Electrochem. Soc.* **2005**, 152, A1763.
- [22] W. Bauer, D. Nötzel, *Ceram. Int.* **2014**, 40, 4591.
- [23] W. Bauer, D. Nötzel, V. Wenzel, H. Nirschl, *J. Power Sources* **2015**, 288, 359.
- [24] L. Ouyang, Z. Wu, J. Wang, X. Qi, Q. Li, J. Wang, S. Lu, *RSC Adv.* **2020**, 10, 19360.
- [25] S. H. Sung, S. Kim, J. H. Park, J. D. Park, K. H. Ahn, *Materials* **2020**, 13, 4544.
- [26] D. Griebel, K. Huber, R. Scherbauer, A. Kwade, *Adv. Powder Technol.* **2021**, 32, 2280.
- [27] F. Ma, Y. Fu, V. Battaglia, R. Prasher, *J. Power Sources* **2019**, 438, 226994.
- [28] A. Basch, R. Horn, J. O. Besenhard, *Colloids Surf., A* **2005**, 253, 155.
- [29] T. Kusano, M. Ishii, M. Tani, O. Hiruta, T. Matsunaga, H. Nakamura, *Adv. Powder Technol.* **2020**, 31, 4491.
- [30] M. Wilhelm, *Macromol. Mater. Eng.* **2002**, 287, 83.
- [31] W. B. Hawley, J. Li, *J. Energy Storage* **2019**, 25, 100862.
- [32] M. L. Williams, R. F. Landel, J. D. Ferry, *J. Am. Chem. Soc.* **1955**, 77, 3701.
- [33] J. D. Ferry, *Viscoelastic Properties of Polymers*, Wiley, <http://books.google.co.uk/books?id=9dqQY3Ujsx4C> (accessed: May 2022).
- [34] CDRheo: Performs Fourier Transform on LAOS rheology data, <https://sourceforge.net/projects/cdrheo/> (accessed: August 2022).
- [35] L. F. Pease, R. C. Daniel, C. A. Burns, *Chem. Eng. Sci.* **2019**, 199, 628.
- [36] D. Lootens, P. Hébraud, E. Lécolier, H. Van Damme, *Oil Gas Sci. Technol.* **2004**, 59, 31.
- [37] I. M. Krieger, T. J. Dougherty, *Trans. Soc. Rheol.* **1959**, 3, 137.
- [38] S. Torquato, T. M. Truskett, P. G. Debenedetti, *Phys. Rev. Lett.* **2000**, 84, 2064.
- [39] W. Pabst, E. Gregorová, C. Berthold, *J. Eur. Ceram. Soc.* **2006**, 26, 149.
- [40] H. Brenner, *Int. J. Multiphase Flow* **1974**, 1, 195.
- [41] R. H. Ewoldt, A. E. Hosoi, G. H. McKinley, *J. Rheol.* **2008**, 52, 1427.
- [42] S. Khandavalli, J. P. Rothstein, *Rheol. Acta* **2015**, 54, 601.
- [43] S. J. Sim, S. H. Lee, B. S. Jin, H. S. Kim, *Sci. Rep.* **2020**, 10, 11114.